Langmuir

Article

pubs.acs.org/Langmuir

Characterizing Pilus-Mediated Adhesion of Biofilm-Forming *E. coli* to Chemically Diverse Surfaces Using Atomic Force Microscopy

He Xu,[†,#] Anne E. Murdaugh,[§,#] Wei Chen,[†] Katherine E. Aidala,[‡] Megan A. Ferguson,[∥] Eileen M. Spain,[⊥] and Megan E. Núñez*[,†]

[†]Department of Chemistry and [‡]Department of Physics, Mount Holyoke College, South Hadley, Massachusetts 01075, United States

[§]Department of Physics, Rollins College, Winter Park, Florida 32789, United States

[∥]Department of Chemistry, State University of New York, New Paltz, New York 12561, United States

[⊥]Department of Chemistry, Occidental College, Los Angeles, California 90041, United States

Supporting Information

ABSTRACT: Biofilms are complex communities of microorganisms living together at an interface. Because biofilms are often associated with contamination and infection, it is critical to understand how bacterial cells adhere to surfaces in the early stages of biofilm formation. Even harmless commensal *Escherichia coli* naturally forms biofilms in the human digestive tract by adhering to epithelial cells, a trait that presents major concerns in the case of pathogenic *E. coli* strains. The laboratory strain *E. coli* ZK1056 provides an intriguing model system for pathogenic *E. coli* strains because it forms biofilms robustly on a wide range of surfaces.*E. coli* ZK1056 cells spontaneously form living biofilms on polylysine-coated AFM cantilevers, allowing us to measure quantitatively by AFM the adhesion between native biofilm cells and substrates of our choice. We use these biofilm-covered cantilevers to probe *E. coli* ZK1056 adhesion to five substrates with distinct and well-characterized surface chemistries, including fluorinated, amine-terminated, and PEG-like monolayers, as well as unmodified silicon wafer and mica. Notably, after only 0−10 s of contact time, the biofilms adhere strongly to fluorinated and amine-terminated monolayers as well as to mica and weakly to "antifouling" PEG monolayers, despite the wide variation in hydrophobicity and charge of these substrates. In each case the AFM retraction curves display distinct adhesion profiles in terms of both force and distance, highlighting the cells' ability to adapt their adhesive properties to disparate surfaces. Specific inhibition of the pilus protein FimH by a nonhydrolyzable mannose analogue leads to diminished adhesion in all cases, demonstrating the critical role of type I pili in adhesion by this strain to surfaces bearing widely different functional groups. The strong and adaptable binding of FimH to diverse surfaces has unexpected implications for the design of antifouling surfaces and antiadhesion therapies.

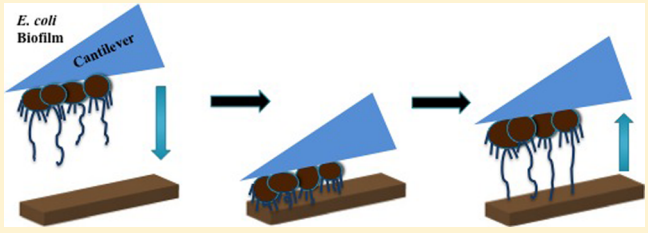

INTRODUCTION

Bacterial biofilms are complex, matrix-enclosed microbial communities that adhere to and proliferate at surfaces.[1] Though biofilms were initially viewed as a peculiar subcategory of bacterial life, it has become clear that complex interfacial communities of microorganisms are common in diverse ecosystems, representing one stage in a biological cycle that also includes the free-swimming planktonic cells most often cultured in the laboratory.[2] Biofilms are characterized by increased resistance to shear forces, chemicals, antibiotic agents, host defense mechanisms, and other stressors.[3−5] This robustness is a critical factor in biofilm-related infections and biofouling in medical and industrial settings. The negative effects of biofilms on human activities have encouraged diverse research efforts to control them.

Researchers have extensively studied bacterial adhesion to a variety of chemically distinct surfaces on a molecular level.[6] Though the exact mechanisms of bacterial adhesion and resistance are still being elucidated, in general surface hydrophobicity has been shown to promote bacterial adhesion while surface hydrophilicity reduces adhesion, due to the entropic costs of releasing organizing water from the interface. Adhesion is diminished on negatively charged surfaces but increased on positively charged surfaces due to electrostatic repulsion.[7] Specifically, self-assembled monolayers of poly(ethylene glycol) (PEG) and zwitterionic surfaces have been reported to carry short-term resistance against attachment by Gram-positive bacteria such as *Staphylococcus epidermidis* and *Staphylococcus aureus* and Gram-negative bacteria such as *Escherichia coli* and *Pseudomonas aeruginosa*.[7−12] From the bacterial perspective, adhesion can be mediated by a range of cell-surface and excreted biomolecules, including both proteins and polysaccharides. Extracellular polymeric substances (EPS), lipopolysaccharides, pili (fimbrae), and flagella have all been

Received: November 30, 2012
Revised: January 23, 2013
Published: February 19, 2013

implicated in adhesion to surfaces during biofilm formation by different bacteria.[2,4,13]

E. coli is a highly adaptable organism. Its characterized strains include harmless commensal strains in the human gut and classic laboratory model organisms. Other *E. coli* strains flourish as both intra- and extraintestinal pathogens, causing food poisoning, urinary tract infections, and contamination of medical devices.[14] As a major component of the human gastrointestinal fauna, its ability to adhere firmly to the intestinal epithelium promotes survival and, for pathogens, virulence. Analogously, the laboratory strain *E. coli* ZK1056 quickly forms robust biofilms on a variety of surfaces, including poly(vinyl chloride) (PVC), polypropylene, polycarbonate, polystyrene, and borosilicate glass.[15] Mutational studies indicate that type I pili play a critical role in biofilm formation by *E. coli* ZK1056.[15] *E. coli* ZK1056 is closely descended from the common laboratory strain K-12, which has been extensively characterized by geneticists and microbiologists.[16,17] This combination of characteristics establishes *E. coli* ZK1056 as an excellent nonpathogenic model for the study of pilus-mediated biofilm formation by pathogenic *E. coli* strains and other Gram-negative bacteria.

In our previous study, we measured the elasticity and adhesive properties of native bacterial biofilm cells using atomic force microscopy (AFM).[18] Cells were probed by extending and retracting a sharp, pyramidal silicon nitride AFM tip into a bacterial cell. *E. coli* ZK1056 cells adhered to the AFM tip with the largest average force and distance components, as well as the largest average number of adhesion events, among all of the cells tested. In this project, we investigate further the chemistry and biophysics of *E. coli* ZK1056 biofilm adhesion. Using atomic force microscopy, we explore quantitatively the adhesion between native ZK1056 biofilms grown on AFM cantilevers and a series of chemically well-defined surfaces, with a focus on the chemical interactions that promote *E. coli* biofilm adhesion.

MATERIALS AND METHODS

Materials. Growth media, buffers, and solvents were obtained from Sigma-Aldrich or Fisher and used as received. Phosphate-buffered saline (PBS) tablets, albumin (bovine, essentially fatty acid free), and lysozyme (from chicken egg white) were purchased from Sigma-Aldrich. Poly-L-lysine hydrobromide was purchased from MP Biomedicals, LLC. Silicon wafers (100 orientation, P/B doped, resistivity 1−10 Ω·cm, and thickness 450−575 μm) were purchased from International Wafer Service. (Tridecafluoro-1,1,2,2-tetrahydrooctyl)dimethylchlorosilane, *N*-(2-aminoethyl)-3-aminopropyltriethoxysilane (AEAPTES), and 2-(methoxypolyethyleneoxypropyl)trimethoxysilane (PEG) were purchased from Gelest, Inc. Muscovite mica was purchased from Ted Pella, Inc. Methyl α-D-mannopyranoside was purchased from Sigma-Aldrich. *E. coli* ZK1056 (misnamed as 2K1056 in ref 15) was obtained as a generous gift from Roberto Kolter, Harvard University.

Preparation of Chemically Defined Surfaces. Rectangular pieces (1.2 × 1.5 cm) of silicon wafers were cleaned with an oxygen plasma cleaner (Expanded Plasma Cleaner PDC-001, Harrick Plasma) for 15 min. Silanization of clean silicon wafers with fluorosilane was performed in the vapor phase at 70 °C for 24 h using 0.5 mL of tridecafluoro-1,1,2,2-tetrahydrooctyldimethylchlorosilane. Silanization of clean silicon wafers with aminosilane was performed in Schlenk flasks extensively purged with nitrogen to minimize moisture. Silanization was carried out in the vapor phase at 90 °C for 24 h using 0.5 mL of *N*-aminoethyl-3-aminopropyltriethoxysilane (AEAPTES). Silanization of PEG was performed in anhydrous toluene with stirring at room temperature for 48 h using 1 mL of 2-[methoxy(polyethyleneoxy)propyl]trimethoxysilane (PEG) for every 20 mL of toluene. After silanization, the wafers were rinsed thrice each with toluene, ethanol, and Milli-Q water. The samples were dried with a stream of nitrogen gas and cured in an oven at 110 °C for 15 min. Afterward, the integrity of each batch of eight monolayer-covered wafers was confirmed by analyzing five by ellipsometry and contact angle goniometry; the remaining three were analyzed by ellipsometry and used for adhesion measurements. To control for variability in efficiency of silanization, three independent batches of surfaces were prepared for the adhesion measurements, and an additional batch was prepared for the mannoside measurements. If not used immediately, samples were stored desiccated until use. Muscovite mica was freshly cleaved using Scotch tape before use.

Protein and Dextran Adsorption. Substrates were soaked in phosphate buffered saline (PBS, pH 7.4) at room temperature for 2 h. Samples were then immersed in protein solution (albumin or lysozyme) of 1 mg/mL in PBS at 37 °C for 1 h or in dextran solution (MW = 148 000) of 1 mg/mL in PBS at 37 °C for 24 h. At the end of the incubation period, the solution was diluted with PBS (3×), keeping the liquid level above the substrate surfaces at all time. Substrates were then rinsed with Milli-Q water, dried with a stream of nitrogen, and desiccated overnight before characterization by ellipsometry, contact angle goniometry, and atomic force microscopy.

Surface Characterization. Each batch of surfaces was characterized by ellipsometry and contact angle measurements. Ellipsometric measurements were obtained with a Microphotonics EL X-01R ellipsometer. The light source was a He−Ne laser with a wavelength of 632.8 nm. The angle of incidence from the normal to the plane was 70°. The thickness of silane monolayer was calculated by subtracting the measured thickness of clean wafer from that of the silane-functionalized surface. Similarly, the thickness of adsorbed protein and dextran layer was calculated by subtracting the thickness of the underlying wafer and monolayer from that of the protein-and dextran-adsorbed surface. Five measurements were made on various regions on each sample, and the calculated average was reported. Contact angle measurements were made with a Ramé-Hart telescopic goniometer and a Gilmont syringe with a 24-gauge flat-tipped needle. Milli-Q deionized water was used as the probe fluid. Dynamic advancing (θ_A) and receding angles (θ_R) were recorded while the probe fluid was added to and withdrawn from the drop, respectively. Five to eight measurements were obtained on different areas of each sample surface, and five surfaces were characterized from each batch, such that a total of 15 surfaces from three different batches were characterized by contact angle measurement. Atomic force microscopy images were obtained with an Asylum Research MFP-3D atomic force microscope operated in contact mode in air.

***E. coli* Biofilm Growth and Attachment to an AFM Cantilever.** *E. coli* ZK1056 cultures were grown to stationary phase (~10^9 cells/mL) overnight at 30 °C with shaking in Difco Nutrient Broth (3.0 g of beef extract, 5.0 g of peptone L^{-1}). A silicon nitride tipless AFM cantilever (NanoWorld) was sterilized in 95% ethanol for 10 min and air-dried. It was then soaked in 1% poly-L-lysine hydrobromide solution (% w/w) for 2 h, gently rinsed in Milli-Q water, and immersed in 100 μL of the *E. coli* ZK1056 culture for 4 h. Then the cantilever was transferred to 1.5 mL of 1/10 strength nutrient broth to grow overnight at 30 °C before the biofilm probe was used for adhesion measurements by atomic force microscopy.

Adhesion Measurement Using Atomic Force Microscopy. The adhesion forces between *E. coli* biofilms and chemical substrates were quantified using an atomic force microscope (Asylum Research MFP-3D). Adhesion between bare AFM cantilever and all the surfaces, as well as that between poly-L-lysine-treated AFM cantilever and all the surfaces, were measured as controls. The spring constant of each cantilever was calibrated using the method of thermal fluctuation prior to tip modification with *E. coli*,[19] and the spring constants k_{sp} for all of the cantilevers fell within the range of 50−70 pN/nm. Adhesion force curves were obtained by allowing the *E. coli*-covered tipless cantilever to approach the surface at a loading velocity of 2 μm/s until a preset loading force of 5 nN was reached, indicating it had made a tight contact with the surface. After a variable contact time with the surface

dx.doi.org/10.1021/la304745s | *Langmuir* 2013, 29, 3000−3011

(0−10 s), the cantilever was withdrawn from the surface at a velocity of 2 μm/s to obtain a force−distance curve. The distance-axis origin was defined as the point of intimate contact (i.e., beginning of the region of constant compliance). All the force curves were obtained in contact mode at room temperature under a solution of 10 mM HEPES buffer at pH 7.6 containing 5 mM $CaCl_2$. Where applicable, the biofilm probe was subsequently immersed in HEPES buffer supplemented with 100 mM methyl α-D-mannopyranoside for 45 min before adhesion measurement was repeated as described.

In each experiment, force curves were obtained on all five surfaces using a single biofilm-functionalized cantilever to control for small variations between individual biofilms. To control for potential wearing or aging of the cantilevers, the order in which adhesion was measured was randomized as a function of contact time (0−10 s), such that the shortest contact times were not always measured first nor the longest measured last, but there was no evidence that order influenced the results. Thirty force curves were measured for each contact time on each surface, with the surface location moved between measurements to ensure that the probe frequently contacted a fresh section of surface. After each AFM experiment, the biofilm probe was air-dried overnight, sputter-coated with gold, and imaged using a scanning electron microscope (Quanta 200, FEI Co.) to confirm the presence of a confluent *E. coli* biofilm on the end of the cantilever. Because of the potential for variability between different preparations of bacteria or chemically modified surfaces, the entire experiment was repeated three times with independently prepared batches of five surfaces and fresh bacteria-coated cantilevers.

Force curves were compiled and adhesion data were analyzed using Igor Pro (WaveMetrics, Inc., Portland, OR). Thirty representative force curves for each contact time on each substrate were blindly selected from among the three independent experiments for force curve analysis. Adhesion energy was calculated as the integrated area under the retraction force curves using home-coded software. Maximum adhesion force, defined as the lowest point of retraction force curves, was manually measured. Rupture length was manually measured as the distance from the contact point (0 μm) to the point of the retraction force curves where the adhesion force returns to zero. Average of adhesion energy, maximum adhesion force, and rupture length are presented with error bars representing the standard deviation.

RESULTS

Chemical Characterization of Surfaces. For studies of *E. coli* biofilm adhesion, we prepared five substrates with distinct and well-defined surface chemistries whose structures are shown in Figure 1: fluorosilane, aminosilane, mica, PEG, and unmodified silicon wafer. Surfaces differ in their degree of hydrophobicity and net surface charge. Fluorosilane is uncharged and hydrophobic. Aminosilane is positively charged because the end amino groups are largely protonated at the neutral pH of our buffers. In contrast, silicon wafer is negatively charged at pH 7.6. Mica, whose tetrahedral SiO_4 and AlO_4 groups are exposed along the cleavage plane, is also expected to be negatively charged in aqueous solution.[20−23] PEG is uncharged, but each molecule carries 9−12 hydrogen bond-accepting ether groups. Each of the five surfaces was characterized by ellipsometry, contact angle goniometry, and atomic force microscopy to establish its basic chemical properties (Table 1 and Supporting Information Figure 1). As predicted, fluorosilane is the most hydrophobic among all surfaces, evidenced by its large advancing and receding contact angles. All the other surfaces are to varying extents hydrophilic. PEG and aminosilane are moderately hydrophilic whereas mica and wafer are extremely hydrophilic, characterized by very small contact angle. Importantly, the measured thicknesses of fluorosilane, aminosilane, and PEG polymer layers determined by ellipsometry are consistent with the formation of tightly packed monolayers, given the known lengths of the silane molecules.

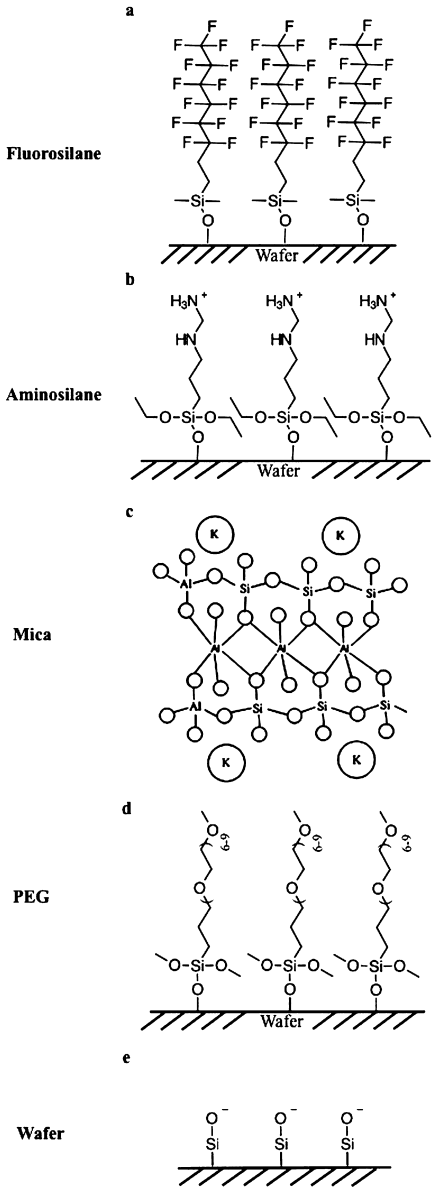

Figure 1. Structures of substrate surfaces. We examined *E. coli* biofilm adhesion to five substrates with distinct and well-defined surface chemistries: fluorosilane, aminosilane, mica, PEG, and unmodified silicon wafer. (a, b, d) Silane monolayers were self-assembled on clean silicon wafer. Amino groups are shown in their protonated ammonium form, as expected in neutral aqueous buffer. (c) Freshly cleaved muscovite mica bears some negative charge in aqueous solution along its cleaved tetrahedral SiO_4 surface (top face) due to the replacement of Si atoms by Al. In this simplified 2-dimensional representation of the crystal, circles represent oxygens or hydroxide groups and formal charges are not shown. (e) Silicon wafer was cleaned using oxygen plasma. The wafer is shown with negatively charged deprotonated silanol groups as expected in neutral aqueous buffer.

Surfaces differ in contact angle hysteresis, the difference between advancing and receding contact angles, a parameter that reflects the physical and chemical heterogeneity of the sample. While wafer and mica are extremely homogeneous, the modified surfaces are less homogeneous evidenced by their much larger contact angle hysteresis. In a complementary

dx.doi.org/10.1021/la304745s | *Langmuir* 2013, 29, 3000−3011

Table 1. Surface Characteristics[a]

	thickness (Å)	roughness (Å)	θ_A (deg)	θ_R (deg)	$\Delta\theta$ (deg)
fluorosilane	6 ± 2	0.8 ± 0.2	106 ± 2	89 ± 4	17 ± 4
aminosilane	6 ± 2	0.9 ± 0.1	51 ± 3	29 ± 3	22 ± 3
mica	NA	0.3 ± 0.1	19 ± 5	13 ± 4	6 ± 2
PEG	8 ± 2	1.0 ± 0.2	38 ± 1	28 ± 1	10 ± 1
wafer	NA	0.5 ± 0.1	4 ± 1	3 ± 1	1 ± 1

[a] θ_A = advancing contact angle; θ_R = receding contact angle; $\Delta\theta$ = contact angle hysteresis.

experiment, the roughness of the silane layers measured by atomic force microscopy is smaller than 1 Å, leading us to conclude that all three surfaces are smooth and well-covered (Table 1).

AFM Measurement of Adhesion Forces between Biofilms and Modified Surfaces. We determined that *E. coli* ZK1056 could initiate biofilm formation on our modified surfaces by incubating each surface in fresh overnight cultures for 5 min or 3 h. After rinsing with distilled water to remove loose cells, surfaces were imaged using contact AFM in air (Supporting Information Figure 2). Large clusters of *E. coli* cells attach to all of the surfaces except PEG in 5 min; there is substantial biofilm formation on all surfaces within 3 h. Given that *E. coli* ZK1056 cells indeed can form biofilms quickly and robustly on chemically diverse surfaces, we quantified the adhesive interaction by utilizing the force measurement modes of the AFM. *E. coli* ZK1056 cells spontaneously grow a native monolayer biofilm on tipless, polylysine-coated AFM cantilevers (Figure 2). After growth in dilute medium, the biofilm-covered cantilevers were rinsed and used without chemical modification to probe the modified surfaces prepared above. Biofilms were maintained in buffer to ensure that the cells remained alive in a native condition while adhesion was measured. Roughly 20 bacterial cells made contact with the substrates during AFM adhesion measurement, as approximated from the dimensions of the cantilever and the loading force of the adhesion measurement, although this number would be expected to vary somewhat from cantilever to cantilever. After force measurements the cantilevers were characterized by SEM to confirm that the biofilm monolayers on the cantilevers remained structurally intact.

During adhesion measurement, the biofilm probes were repeatedly extended to contact the surface, maintained in contact with the surface for a variable period of time (0, 1, 5, or 10 s), and retracted from the surface. Representative retraction force–distance curves for 0 and 10 s contact time on all surfaces are presented here (Figure 3). Retraction force–distance curves for each surface are distinct in terms of the magnitude of the adhesion force, the rupture length of the adhesion events, and the general shape of the force curves.

Force curves obtained on fluorosilane are characterized by an initial, very strong adhesion event followed by a smaller secondary adhesion event (Figure 3a,b). The initial adhesion event is accompanied by a large force component and short (~150 nm) but uniform rupture length. The general force signature is well preserved as the contact time of biofilm probe with the surface is increased. Unusually, the force curves are highly reproducible in shape and magnitude from cycle to cycle.

Force curves on aminosilane are more variable from retraction to retraction, but nonetheless as a group they also share a distinct set of signatures: multiple sawtooth-shaped adhesion events are observed at all locations on the substrate and at all contact times (Figure 3c,d). These "sawtooth" adhesion events have an average force component increasing from around 1 nN to almost 3 nN with prolonged surface contact and a distance component that can extend out to almost 3 μm after 10 s of surface contact. With increased contact time on the substrate, both the magnitude of the adhesion force and the rupture length of these sawtooth adhesion events increase, but the general sawtooth shape is retained.

Force curves on mica are characterized by a large, rounded adhesion event (Figure 3e,f) whose shape contrasts sharply with the well-defined, pointed adhesion events observed on aminosilane. The strong adhesion between probe and sample releases gradually as the biofilm-probe is pulled away from the substrate, giving rise to a slowly diminishing force component with many small "teeth" in the adhesion event. The eventual rupture length is hard to define, as the small "teeth" of adhesion tend to blend in with inherent noise in the force curves.

Very little adhesion is observed upon retraction of the biofilm probe after 0 s contact with PEG, though some adhesion events with extended flat force plateaus occur after 10 s contact (Figure 3g,h). Unmodified wafer demonstrates its resistance to *E. coli* adhesion, as none of the retraction force–distance curves reveals any adhesion event (Figure 3i,j). This lack of adhesion contrasts with the extensive coverage of bacterial biofilms on wafer as seen in bacterial deposition experiments, in which traces of growth medium and more cells are present (Supporting Information Figure 2). Similarly, adhesion events are observed between *E. coli* biofilms and wafers that have not

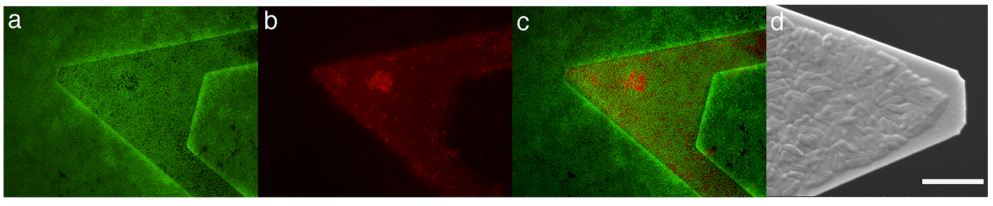

Figure 2. Native *E. coli* biofilms grown on AFM cantilevers. Tipless silicon nitride AFM cantilevers were coated in polylysine, immersed in fresh *E. coli* ZK1056 cultures for 4 h, and transferred to diluted nutrient broth overnight, during which time *E. coli* ZK1056 biofilms formed on the cantilever. (a–c) Biofilm viability was examined using fluorescent staining of control cantilevers. Panel a shows cells stained with green fluorescent SYTO-9, which binds to all cells. Panel b highlights those cells that were stained by red fluorescent propidium iodide, which penetrates only damaged cells. Panel c is the overlay of panels a and b. Though widespread green fluorescence is observed along with some background propidium–polylysine binding, few cells are stained bright red indicating that they have been damaged. (d) To confirm that the biofilms remained intact throughout the experiments and did not peel off or rupture, biofilm cantilevers were routinely imaged by SEM after AFM adhesion measurements. The scale bar corresponds to 5 μm.

dx.doi.org/10.1021/la304745s | *Langmuir* 2013, 29, 3000–3011

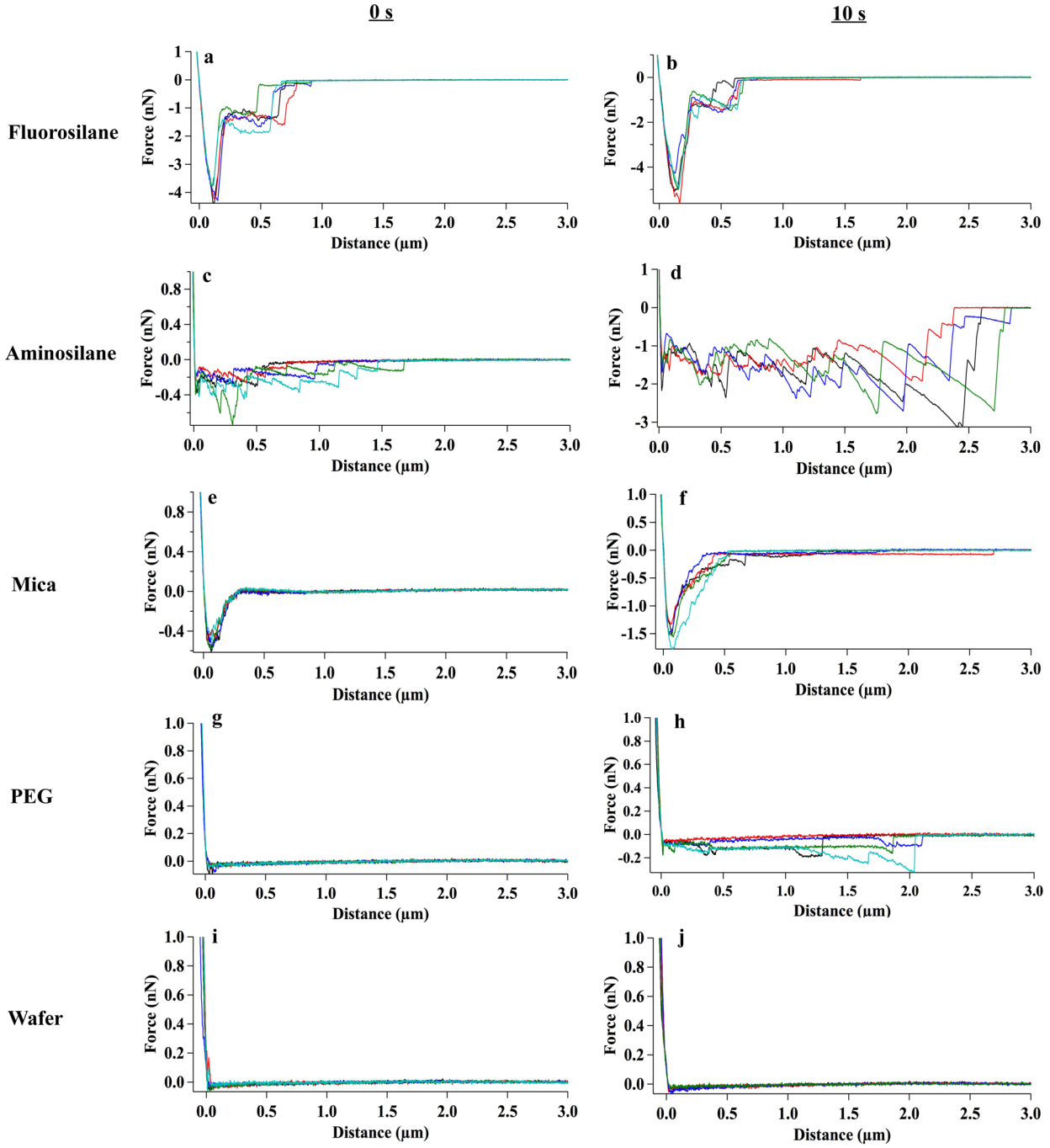

Figure 3. AFM retraction curves showing adhesion between *E. coli* biofilms and five surfaces. The *E. coli* biofilm AFM probe was repeatedly brought into contact with the five substrates, allowed to sit in contact with the surface for a fixed interval between 0 and 10 s, and retracted. The force experienced by the cantilever during retraction is plotted as a function of separation between the substrate and biofilm, with 0 μm representing the initial contact point. Five representative force curves are presented for each substrate, measured at 0 s (left column) and 10 s (right column). Each chemically distinct surface displays a unique pattern of adhesion.

been plasma-cleaned before use (Supporting Information Figure 3), also indicating that organic debris facilitates adhesion.

To better characterize the trends observed in the force curves, we analyzed 30 blindly selected representative retraction force curves for each surface and contact time according to three quantities: adhesion energy, calculated from the integrated area under the retraction force curves; maximum adhesion force, measured as the lowest point of the retraction force curves; and rupture length from origin, measured as the distance between the point of origin and the point where adhesion returns to zero (Figure 4). For all periods of contact time with substrate, fluorosilane demonstrates the largest degree of adhesion energy, followed by aminosilane, mica, PEG, and wafer (Figure 4a). Adhesion energy generally increases as a function of contact time on all substrates. The largest maximum adhesion force is also observed on fluorosilane, followed by aminosilane and mica (Figure 4b). Small adhesion is observed on PEG, and zero adhesion is observed on wafer. No adhesion is also measured between any

dx.doi.org/10.1021/la304745s | *Langmuir* 2013, 29, 3000−3011

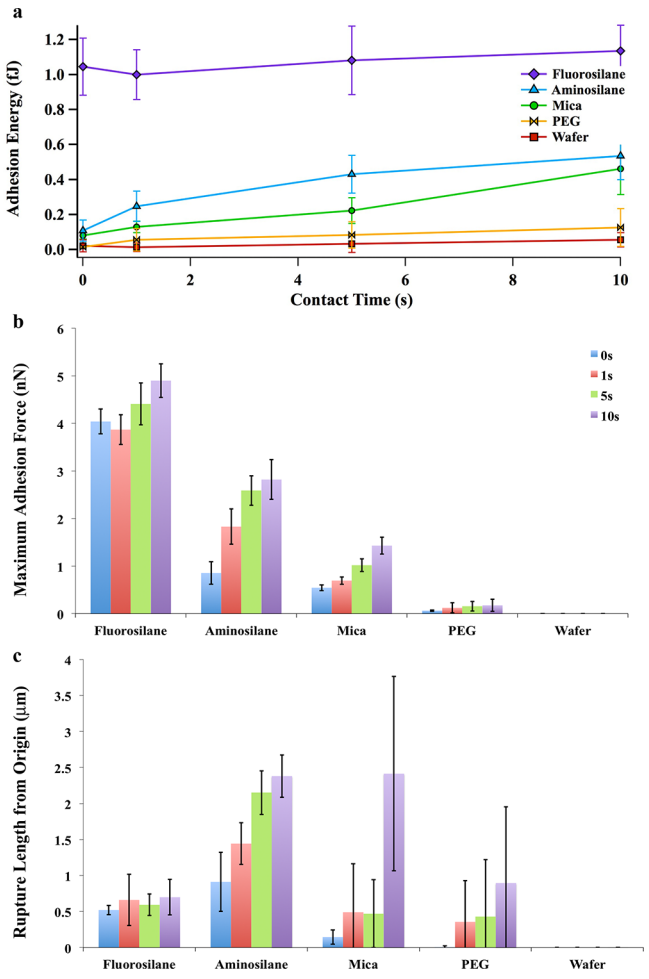

Figure 4. *E. coli* biofilm adhesion to five surfaces as a function of contact time. The distinct shapes of the adhesion force vs distance curves measured between *E. coli* biofilms and different substrates can be analyzed according to various metrics. (a) Adhesion energy is calculated from the integrated area under the retraction force curves. (b) Maximum adhesion force is defined as the lowest point of the retraction force curves. (c) Rupture length from origin is defined as the distance from the contact point (0 μm) to the point of the retraction force curves where the adhesion force returns to zero. Though the adhesion energy, force, and length all generally increase as a function of contact time, the trends between surfaces vary depending on the metric used to define adhesion. Error bars represent one standard deviation calculated from 30 blindly selected force curves measured with three different cantilevers.

of the surfaces and control cell-free poly-L-lysine-coated probes (Supporting Information Figure 4). On all substrates (except wafer) the maximum adhesion force increases with prolonged contact with the substrate. Notably, the magnitude of the adhesion forces varies considerably among the different types of surfaces: on fluorosilane and aminosilane, the maximum adhesion forces are on the order of a nanonewton, whereas for mica the adhesion force starts out on the piconewton scale but increases beyond the nanonewton threshold as contact time is increased. On the other hand, PEG maintains piconewton maximum adhesion forces from 0 to 10 s contact.

The magnitudes of the adhesion energies and forces are proportional to the number of cells and biomolecules that contact the surface, but the exact number of cells in contact with the surface is difficult to measure, so we cannot determine the energy of individual biomolecule−surface or cell−surface interactions. Thus, the trends in energies and forces, not the absolute magnitudes, are most relevant to consider.

The rupture length from origin provides an estimate of how far the interaction between biofilm and substrate extends away from the substrate due to the types of biomolecules involved in the adhesion process. A trend across substrates is much less distinct than in the case of maximum adhesion force. Fluorosilane has the smallest average rupture length, below 1 μm, while aminosilane and mica are characterized by the largest rupture lengths overall, around 2.5 μm at the longest contact times (Figure 4c). While the rupture length is not affected by increased contact time on fluorosilane, it increased from 0 to 10 s contact on all the other substrates, though accompanied by large curve-to-curve variability in the case of mica and PEG. Error bars representing the standard deviation are much greater than those for maximum adhesion force, as the differences in force−distance curve shape between samples, including the presence of sawtooth-shaped adhesion events and the extended force plateaus mentioned previously, introduce inconsistencies in the definition of rupture length. In the case of curves with multiple overlaid snap-off events (particularly with mica or aminosilane), the length represents the longest possible extension (*vide infra*). As a result, the rupture lengths should be used only as a rough approximation of biomolecule length.

Protein Deposition. In order to relate biofilm adhesion behavior to the biomolecules most likely to mediate *E. coli* biofilm adhesion, we examined deposition behavior of model proteins onto our five substrates to see if there was a correlation between biomolecule adsorption and biofilm adhesion. Surfaces were first immersed in a solution of albumin or lysozyme for 1 h before being thoroughly rinsed, dried, and characterized using ellipsometry, contact angle goniometry, and atomic force microscopy (Figure 5 and Supporting Information Figure 1). The thickness measured by ellipsometry serves as an indirect measure of the extent of coverage by proteins on the surface. Fluorosilane shows the highest degree of protein adsorption. Aminosilane presents a moderate and differential degree of protein adsorption, with the amount of albumin adsorption higher than that of lysozyme. This pattern indicates that electrostatic binding plays a significant role in deposition because albumin has a net negative charge and lysozyme a net positive charge at this pH. The thickness on mica could not be obtained by ellipsometery. PEG demonstrates little, if any, protein adsorption evidenced by the measured negligible protein layer thickness. Wafer also shows a highly differential pattern of protein adsorption, with negligible albumin adsorption but significant lysozyme adsorption, correlating with predicted electrostatic effects.

A coating of protein changes the apparent hydrophobicity/hydrophilicity of a surface as evidenced by the advancing and receding contact angles. Albumin and lysozyme adsorption decrease surface hydrophobicity of fluorosilane and increase the hydrophobicity of mica (Figure 5b,c). Albumin and lysozyme bind differently to aminosilane and unmodified wafer as predicted by electrostatics: positively charged aminosilane is bound preferentially by negatively charged albumin, while negatively charged wafer prefers positively charged lysozyme.

Consistent with the ellipsometry data, the substrate contact angle hysteresis is significantly larger after protein adsorption except in the case of PEG, which is resistant to protein adsorption (Figure 5d). This increase indicates increased surface roughness and chemical heterogeneity upon protein

dx.doi.org/10.1021/la304745s | *Langmuir* 2013, 29, 3000−3011

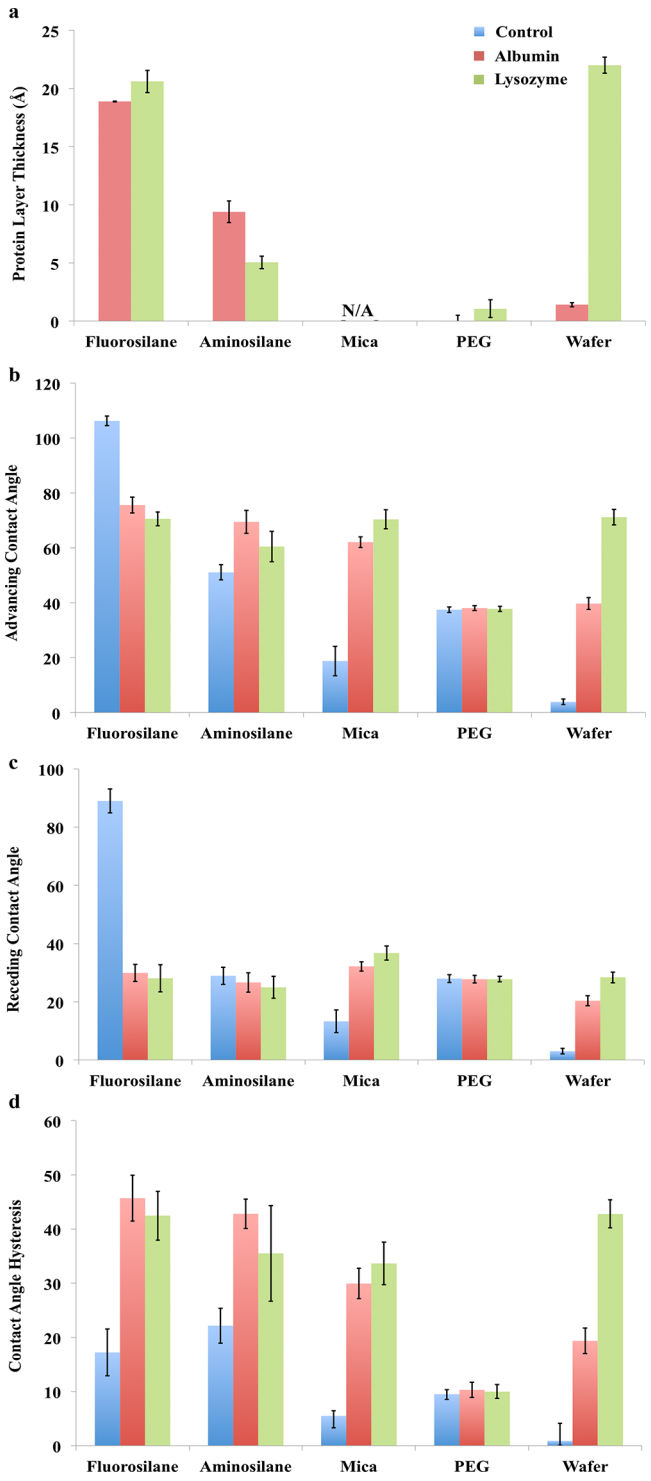

Figure 5. Protein adsorption on five surfaces. Substrates were immersed in solutions of albumin or lysozyme to explore adsorption of protein as a function of surface chemistry. Substrates were immersed in protein solutions (1 mg/mL in PBS) at 37 °C for 1 h before being rinsed, dried, and characterized by ellipsometry and contact angle goniometry as follows: (a) protein layer thickness; (b) advancing contact angle; (c) receding contact angle; (d) contact angle hysteresis. In all cases, blue represents the buffer control, red bars albumin, and green bars lysozyme. At neutral pH, albumin is expected to carry a net negative charge and lysozyme a net positive charge.

adsorption on smooth underlying substrates. While albumin and lysozyme change the measured hysteresis of fluorosilane, aminosilane, and mica to similar extents, a large protein-dependent difference is seen in the case of wafer, as albumin appears to deposit poorly on wafer as compared to lysozyme.

Overall, the pattern of albumin adsorption corresponds well with the trends in biofilm adhesion (largest on fluorosilane, moderate on aminosilane and mica, and minimal on PEG and wafer), but the pattern of lysozyme adsorption follows a slightly different trend. The polysaccharide dextran also adsorbs to the modified surfaces, but with trends distinct from that of bacterial adhesion (Supporting Information Figure 5).

Methyl α-D-Mannopyranoside Inhibition of Biofilm Adhesion. Given the large distance component in many of the retraction force curves, we explored whether *E. coli* ZK1056 biofilm adhesion was mediated via pili, long proteinaceous cell surface appendages common on many *E. coli* strains that we have observed directly on ZK1056 (Supporting Information Figure 6).[18,24] We measured biofilm adhesion to our five surfaces before and after 45 min incubation of the biofilm cantilevers with the nonhydrolyzable mannose analogue methyl α-D-mannopyranoside (mannoside), which inhibits the terminal adhesin FimH on type I pili. Notably, mannoside significantly reduces adhesion to all substrates as evidenced by the striking decrease in adhesion energy and maximum adhesion force (Figure 6a,b). Rupture length from the origin is reduced on aminosilane, mica, and PEG, but not on fluorosilane where the mean rupture length is maintained around 500 nm (Figure 6c).

It should be noted that the adhesion magnitudes measured before mannoside addition were significantly larger in this experiment than in Figure 4 in that fluorosilane adhesion is very large and adhesion on wafer is not zero. Clearly, changes in the number of biomolecules contacting the surface (due to slightly different numbers of cells, expression of biomolecules, or cantilever angles between days) can sensitively affect the overall magnitudes of the measured adhesion forces and energies. Nonetheless, the trends in energies and forces are essentially the same. That mannoside can substantially inhibit biofilm–surface binding was confirmed on three occasions with unique biofilm cantilevers and modified surfaces. SEM images confirmed the integrity of the biofilm on the cantilever after incubation with mannoside and AFM force measurements (Supporting Information Figure 7). We investigated the possibility that mannoside interferes with adhesion indirectly by coating the surfaces, but no changes in contact angle were observed on any surface after incubation with mannoside (Supporting Information Figure 8).

DISCUSSION

Preparation of Biofilm Probes and Chemically Distinct Surfaces. Here we used the force measurement modes of the AFM to explore the chemical and physical characteristics of adhesion by the nonpathogenic laboratory strain *E. coli* ZK1056, a robust biofilm former. Previously, we measured the adhesion of *E. coli* ZK1056 cells to silicon nitride AFM tips, demonstrating that these cells were significantly more adhesive than *E. coli* ML35, *Micrococcus luteus*, *Pseudomonas putida*, and *Bacillus subtilis* cells, in terms of both the strikingly large forces (1.2 ± 0.7 nN) and lengths (1.4 ± 1.0 μm) associated with the adhesion events in the retraction curves.[18] We hypothesized that multiple cell surface macromolecules could attach to the retracting AFM tip. However, because the AFM tip is sharply pointed, we were unable to rule out the possibility that the tip punctured the bacterial cells and on retraction pulled out large portions of the cell membrane, peptidoglycan, or cytoplasmic

dx.doi.org/10.1021/la304745s | *Langmuir* 2013, 29, 3000–3011

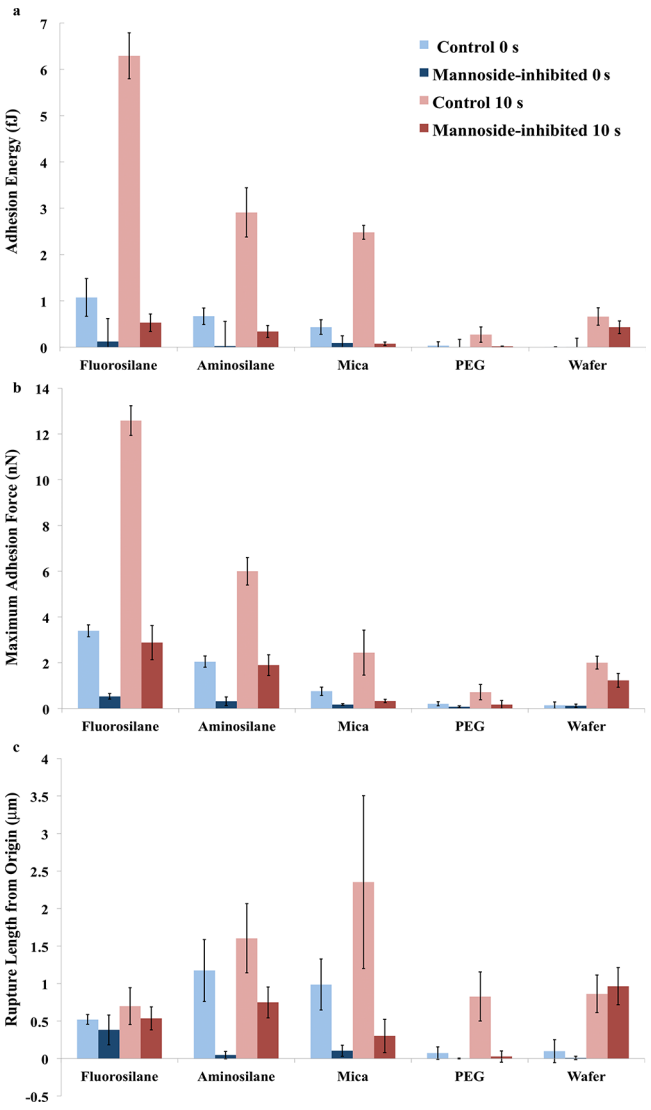

Figure 6. Inhibition of *E. coli* biofilm adhesion to surfaces by methyl α-D-mannopyranoside. Adhesion forces between an *E. coli* biofilm-covered probe and the surfaces were measured from AFM retraction curves, similar to Figures 3 and 4. To explore inhibition of adhesion by type I pili, biofilm probes were then incubated with 100 mM methyl α-D-mannopyranoside, a FimH inhibitor, for 45 min before adhesion was measured again. Curves were analyzed in terms of the following metrics: (a) adhesion energy; (b) maximum adhesion force; (c) rupture length from origin. Blue bars display the adhesion after 0 s, and red bars display adhesion after 10 s. In each pair of red or blue, light bars show the control biofilm samples and dark bars the biofilms preincubated in methyl α-D-mannopyranoside.

components. In the experiments described here, we have inverted the experimental setup such that the pointed tip is entirely absent, having been replaced by a flat, biofilm-coated cantilever so that only the biofilm cell surfaces can contact the test substrate.

It can be challenging to bind cells to the cantilever such that they do not peel off during the experiment. Several groups have immobilized bacterial cells to cantilevers by chemical fixation with glutaraldehyde, but such chemical fixation can modify the elastic and adhesive properties of Gram-negative bacterial outer membranes.[25−30] A better method is to adhere cells to a polylysine-coated cantilever, foregoing the glutaraldehyde.[31−34] We grew living *E. coli* ZK1056 biofilms on polylysine-coated cantilevers (Figure 2), allowing us to explore the adhesion of *E. coli* biofilms under near-native conditions. We confirmed the viability of the cells on the polylysine-coated cantilever using fluorescence microscopy (Figure 2a−c). Bacteria did not adhere sufficiently strongly to the cantilevers in the absence of polylysine for us to carry out force measurements without it, but we expect its effect on cell surface properties to be modest.[35] Importantly, when we carried out AFM adhesion controls with the parent *E. coli* strain K12 and the laboratory "cousin" ML35, these bacterial cells quickly peeled off of the cantilever surface (data not shown). This clear difference in the robustness and integrity of the biofilms formed by the common laboratory strains versus ZK1056 emphasizes the adhesive properties of the latter.

This inverted geometry has the added benefit that it is straightforward to prepare modified substrates with defined chemistries and characterize them extensively (Table 1). Using contact angle goniometry, ellipsometry, and AFM, we confirmed that the silanes form self-assembled monolayers on silicon wafer, and these monolayers are flat, densely packed, and relatively uniform. Critically, our measurements of surface hydrophobicity and layer thickness are fully consistent with the molecular structures, so we can be confident in our descriptions of the surface chemistry. The disadvantage to this method is that the absolute magnitudes of the observed adhesion forces and energies will depend on the number of cells contacting the surface, a number that is difficult to control exactly, and thus the strengths of individual biomolecular interactions cannot be determined.

AFM Measurement of Adhesion Forces between Biofilms and Modified Surfaces. When the Kolter lab explored biofilm formation by *E. coli* K12 descendants, they discovered *E. coli* ZK1056 to be an extremely strong biofilm former on a variety of surfaces. We previously observed using crystal violet staining and AFM that *E. coli* ZK1056 quickly forms thick biofilms on glass coverslips, even in dilute medium.[18,24] Here we confirmed that *E. coli* ZK1056 is indeed a very adhesive strain by screening for spontaneous bacterial attachment to five chemically distinct surfaces (Supporting Information Figure 2). Despite the overall strong binding to surfaces bearing different functional groups, the trend of ZK1056 attachment is consistent with previous studies of bacterial deposition: it attaches most quickly and robustly to the hydrophobic fluorosilane surface, less thoroughly to the charged surfaces, and most slowly and weakly to the hydrophilic, H-bond-accepting PEG.[6−12,36−41] Even though the ZK1056 cells bear a substantial net negative charge according to zeta potential measurements (data not shown), they show no strong preference for the positively charged aminosilane over the negatively charged mica and wafer surfaces; clearly, electrostatic attraction plays a minor role in attachment in buffer due to screening by ions. The cells are also able to attach to both mica and wafer despite the exceptionally smooth texture of both surfaces, supporting the idea that surface roughness is not required for firm attachment.

To examine more deeply the chemistry of attachment, we used AFM to quantitatively measure the adhesion forces between biofilms and surfaces. After being pressed to a surface and allowed 0−10 s of contact time, *E. coli* ZK1056 biofilms adhere most strongly to hydrophobic fluorosilane, in terms of both maximum energy and force. Biofilms adhere less strongly to charged, hydrophilic aminosilane and mica, weakly to uncharged hydrophilic PEG, and not at all to negatively charged

dx.doi.org/10.1021/la304745s | *Langmuir* 2013, 29, 3000−3011

silicon wafer. With the exception of bare wafer, this trend is roughly consistent with the spontaneous bacterial attachment on longer time scales. Adhesion to unmodified wafer appears to depend critically on the presence of organic debris (largely absent in the AFM experiments), consistent with data that a preadsorbed protein "conditioning film" on surfaces facilitates subsequent adhesion by bacteria (Supporting Information Figure 3).[11] In the absence of mediating organic molecules, the electrostatic repulsion between bacterial cells and wafer prevents adhesion. In sharp contrast, on mica screened by buffer cations Ca^{2+} and Na^{+},[22,23,42] electrostatic repulsion between cells and mica is negligible and adhesion is strong.

Adhesive Proteins on the Surfaces of *E. coli* Biofilms. The retraction curves provide provocative clues about the source of ZK1056's avid biofilm-forming ability. Adhesion events on aminosilane, mica, and PEG are characterized by long distance components, often extending beyond 1 μm and increasing as a function of contact time. Remarkably, these distances are consistent with the adhesion components of retraction that we previously measured using sharp silicon nitride tips on ZK1056 cells.[18] Two classes of polymers are available to bind to the substrates: sugars (including exopolysaccharides or lipopolysaccharides) or proteins (including cell surface proteins such as porins and extracellular proteinaceous structures like flagella and pili). Biochemical characterization of ZK1056 and its parent strain K12 in our lab demonstrates that both K12 and ZK1056 are "rough strains", meaning that the lipopolysaccharides on the surface of the cells have severely truncated polysaccharides that can only extend a short distance (Supporting Information Figure 9). Some excreted exopolysaccharides (EPS) are observed in ZK1056 biofilms, but we expect the layer of EPS to be modest given the short growth time, dilute medium, small number of cells, and thorough rinsing before use. Also, K12 cannot form anchored capsules of EPS due to its truncated LPS.

Thus, proteins likely make a major contribution to the large adhesion forces. We examined the deposition of two proteins, lysozyme and albumin, onto the five chemically distinct surfaces for similarities to the trends in biofilm adhesion (Figure 5) as well as the deposition of dextran as a polysaccharide model for EPS (Supporting Information Figure 5). The pattern of albumin deposition best corresponds to the pattern in biofilm adhesion forces/energies: high for fluorosilane, modest for aminosilane and mica, low for PEG and wafer, consistent with the published literature outlining the entropic and electrostatic effects on protein adhesion.[43−46] On the basis of this comparison, we hypothesize that a surface protein with a negatively charged face similar to albumin plays a major role in adhesion by this strain; other proteins and EPS appear to play smaller roles.

The most likely candidate proteins involved in adhesion are outer membrane proteins or long proteinaceous appendages. A major protein family found in the outer membrane of Gram-negative bacteria are porins, transmembrane β barrel proteins that allow the passage of small solutes into the periplasm. A β barrel protein of roughly 400 amino acids has a length of ∼150 nm upon full extension. Thus, the measured extensions of 1 μm or more cannot be mapped directly to the extension of a porin molecule, though we cannot exclude the possibility that a composite of porin extension and cell deformation might account for the adhesion lengths we observe.

We have previously demonstrated the presence of long proteinaceous cell surface appendages, both flagella and pili, on the surface of ZK1056 cells using AFM (Supporting Information Figure 6).[18,24] Pratt and Kolter used genetic and microbiological techniques to show that *E. coli* ZK1056 bearing inactive type I pili (either mutated or inhibited with methyl α-D-mannopyranoside) could no longer form biofilms on plastic or glass surfaces, whereas flagellar mutants could still form biofilms, albeit not as robustly.[15] We measured *E. coli* ZK1056 adhesion to our five substrates after incubation with methyl α-D-mannopyranoside, and in all cases, the force and energy of adhesion were decreased. Lengths of adhesion were also dramatically decreased, except in the case of wafer.

The inhibition of biofilm adhesion points strongly to type I pili as a major contributor to biofilm adhesion to chemically distinct substrates. Type I pili are proteinaceous adhesive structures composed of 1−2 μm long helical rods of FimA protein subunits.[47,48] Each pilus is capped by a FimH protein that binds mannose strongly, allowing the *E. coli* cells to bind to gastrointestinal cell surfaces and other glycan-decorated mammalian cells. The mannose-specific binding site has presented an appealing target for pharmacological investigation, resulting in somewhat contradictory predictions about the valency and specificity of binding.[49] Crystal structures of FimH have been obtained with mannose analogues showing the mannose-specific binding site,[50] but this does not exclude the possibility of binding sites for other chemical groups. Interestingly, none of our chemically modified substrates strongly resembles mannose. In conjunction with the findings of Pratt and Kolter, our data support alternative nonspecific binding partners for this protein besides mannose. Furthermore, they point to the importance of multiple weak nonspecific interactions in generating strong adhesion by whole cells or small clumps of cells. Strong adhesion by these small model biofilms containing only ∼20 bacteria illustrates how nonspecific interactions (weak on an individual scale but occurring in a coordinated fashion on a biological surface) might have profound relevance in environmental and medical settings where individual bacteria and small clusters of bacteria can break off of biofilms and colonize distant surfaces.

The primary adhesion components of the retraction curves on fluorosilane are much shorter (∼150 nm) than those on mica, PEG, and aminosilane; the secondary events are almost always less than 1 μm long and do not increase with contact time. Given fluorosilane's hydrophobicity and inability to form hydrogen bonds, the biofilm adhesion likely is dominated by hydrophobic interactions, where the large adhesion event corresponds to the exclusion of water at the interface between the fluorosilane and the biofilm surface. Nonetheless, inhibition of FimH reduces adhesion to fluorosilane, indicating that pili play some role even in adhesion to highly hydrophobic surfaces.

Analyzing the Shape of Adhesion Force Curves. The variation in the shapes of the force curves leads us to consider the factors that contribute to their shapes. When a relaxed, disordered polymer is stretched, there is an initial extension at constant, low force corresponding to pulling the polymer out to a linear form (the "entropic regime"), followed by a second nonlinear regime when the extended polymer is stretched in a springlike fashion requiring increasing force. When the polymer is released or broken, referred to as the "snap-off", the force sharply returns to a smaller value. This extension of linear biopolymers has been described mathematically according to relatively simple models, such as a wormlike chain (WLC) or freely jointed chain (FJC) models, which describe biomolecules as continuous chains of homogeneous and noninteracting

segments.[51−55] Extensions of isolated single biomolecules have been measured by AFM and optical tweezers, and the force−distance curves display this generalized polymer extension behavior. We fitted WLC and FJC models to isolated adhesion to determine whether the contour length was more similar to that of pili or of membrane proteins. While the persistence length obtained by these fits was within the range expected for proteins (on the order of the 0.38 nm Cα to Cα distance), the contour length varied between the models. There are several reasons why polymer extension models might not fully explain the stretching of multiple biomolecules from a cell surface. Hydrophobic, electrostatic, and hydrogen-bonding interactions within real proteins are explicitly discounted in simple polymer models, leading to difficulties in establishing a persistence length and in fitting the shape of an ideal polymer stretching curve to a real one. More seriously, since the cells can stretch and distend as the biofilm is pulled away from the surface, a large portion of the retraction curve may reflect cellular deformation and not protein stretching. Thus, although we were able to fit adhesion events and obtain values for persistence length and contour length, the model could not conclusively identify our biomolecule as a pilus. Other groups have also seen that simple polymer models fail to describe some of the complexities of protein extension from a cell surface.[34,56]

Despite the difficulties, a polymer stretching model still qualitatively describes the shapes of the adhesion force curves measured when the biofilm is retracted from a surface. Several additional factors influence the shape of the curve. First, ordered protein folds can be dramatically changed as a protein is stretched and the bonds between structural units fail cooperatively, yielding an extended, denatured protein. The loss of packed globular structure leads to sudden decreases in force with increasing length, as other groups have shown for Titin, GPF, immunoglobulin, fibronectin, and OmpA.[53,57,58] These changes in protein folding and packing, seen as sharp decreases in measured force as the polymer length increases, make the retraction curve appear jagged (with the size of the teeth depending on the energy of unfolding). On our adhesion curves measured on all surfaces, we frequently observe small, jagged teeth that are likely to correspond to unfolding of protein structure. The repeating FimA subunits of pilin are coiled into a hollow helix; when stretched, the helix has been observed to unravel without breaking, allowing the pilus to become significantly longer.[59−61] The shape of the published retraction curves measured on isolated pili bears striking similarity to the plateau-shaped curves we observe with PEG and with mica at longer extensions and also to the small (<150 nN) jagged features we observe in the midst of our more complicated retraction curves.

A second factor influencing the shape of the retraction curve is the strength of attachment between the biomolecule and the surface. If the attachment is weak, the polymer will be straightened out (extended antientropically) only slightly before it releases from the retracting surface, leading to a plateau-shaped retraction curve at relatively low forces. If the attachment is strong, however, the polymer will be stretched significantly before it releases from the retracting surface, leading to a pronounced "sawtooth"-shaped retraction curve with a large measured force component. That is, the same molecule can be characterized by an apparently different retraction curve if its attachment to the surface is significantly different. *E. coli* ZK1056 biofilm adhesion to PEG is characterized almost exclusively by plateau-shaped curves, consistent with weak attachment to the PEG surface, whereas the retraction curves on aminosilane have large, sawtooth-shaped events consistent with very strong adhesion.

One of the most striking aspects of our retraction force curves is the magnitude of the measured adhesion (Figures 3 and 4). The nanonewton-scale forces are far too large to correspond to an individual biomolecule−surface interaction; receptor−ligand interactions or protein unfolding events would be expected to occur in the range of tens to hundreds of piconewtons.[62] Nanonewton-scale forces are consistent with other measurements of adhesion between bacteria-covered AFM tips and surfaces.[25,26,29−31] Thus, the magnitudes of the force components of the adhesion curves shown here argue convincingly that multiple bonds are formed between the surface and the biofilm, consistent with our estimate that ∼20 bacterial cells contact the surface at once. In the case of mica, it appears that these bonds work together additively, releasing incrementally as the distance is increased. Similarly shaped curves were observed for multiple type I pili extended simultaneously with silicon nitride AFM tips.[60] Conversely, in the case of aminosilane, the bonds appear to work together cooperatively, releasing in large, nanonewton-scale "snap-off" events that are too large to correspond to a single interaction.

Taken together, these considerations may begin to explain the surprising diversity of adhesion distances, forces, and retraction curve shapes observed for the adhesion between *E. coli* ZK1056 biofilms and chemically distinct surfaces, and they raise fascinating new questions for further exploration.

CONCLUSIONS AND IMPLICATIONS

In this work, we explored the adhesion of the nonpathogenic laboratory strain *E. coli* ZK1056. This strain adheres quickly and robustly to surfaces displaying a range of chemical functionalities, including hydrophobic fluorosilane, positively charged aminosilane, and negatively charged mica. These strong biofilm formers can even adhere to antibiofouling PEG surfaces, albeit more weakly and slowly, and to bare silicon wafer if mediated by proteins. Clearly, these cells are capable of multiple responses and are adaptable to many different kinds of surfaces, combining many nonspecific interactions to adhere quickly and strongly to hydrophobic and hydrophilic surfaces. From the perspective of those trying to design an antifouling biocompatible surface, the ability of these bacteria, and the pathogenic *E. coli* strains for which they serve as a model, to bind avidly to such a wide variety of functional groups is daunting to say the least.

Nonetheless, the inhibition of type I pili, and specifically the binding pocket of FimH, dramatically reduces adhesion of these robust biofilm-forming bacteria to surfaces, even when the substrates bear no similarity to mannose. It is apparent that in our efforts to prevent biofilm formation we must think more broadly about the "mannose" binding site, FimH inhibition, and adhesion by type I pili.

ASSOCIATED CONTENT

Supporting Information

AFM images of modified surfaces, bacterial cell deposition onto surfaces imaged by AFM, an SEM image of a mannose-modified biofilm probe, AFM image of ZK1056 showing pili, deposition of dextran onto modified surfaces, contact angle and thickness of mannose deposited on surfaces, retraction curves on unclean wafer, adhesion energies of bare poly-L-lysine probes on modified surfaces, and a lipopolysaccharide

characterization gel. This material is available free of charge via the Internet at http://pubs.acs.org.

AUTHOR INFORMATION

Corresponding Author

*E-mail menunez@mtholyoke.edu; Ph (413) 538-2449; Fax (413) 538-2327.

Author Contributions

#Both authors contributed equally to this work.

Notes

The authors declare no competing financial interest.

ACKNOWLEDGMENTS

We thank Professor Roberto Kolter of Harvard University for his generous gift of *E. coli* ZK1056, Terri Camesano and her students for helping us to measure zeta potentials, and Catherine Volle for sharing her characterization data for *E. coli* ZK1056 lipopolysaccharides. We are deeply grateful to Emma Hughes and Marian Rice for their assistance with fluorescence microscopy. This work was supported by the National Science Foundation (CHE-0910578), the Howard Hughes Medical Institute, the Clare Boothe Luce Foundation, and the Camille and Henry Dreyfus Foundation.

REFERENCES

(1) Karatan, E.; Watnick, P. *Microbiol. Mol. Biol. Rev.* **2009**, *73*, 310−347.
(2) Stoodley, P.; Sauer, K.; Davies, D. G.; Costerton, J. W. *Annu. Rev. Microbiol.* **2002**, *56*, 187−209.
(3) Parsek, M. R.; Singh, P. K. *Annu. Rev. Microbiol.* **2003**, *57*, 677−701.
(4) Costerton, J. W.; Stewart, P. S.; Greenberg, E. P. *Science* **1999**, *284*, 1318−1322.
(5) Vertes, A.; Hitchins, V.; Phillips, K. S. *Anal. Chem.* **2012**, *84*, 3858−3866.
(6) Katsikogianni, M.; Missirlis, Y. *Eur. Cells Mater.* **2004**, *8*, 37−57.
(7) Cunliffe, D.; Smart, C. A.; Alexander, C.; Vulfson, E. N. *Appl. Environ. Micobiol.* **1999**, *65*, 4995−5002.
(8) Holmberg, K.; Bergstrom, K.; Brink, C.; Osterberg, E.; Tiberg, F.; Harris, J. M. *J. Adhes. Sci. Technol.* **1993**, *7*, 503−517.
(9) Kingshott, P.; Wei, J.; Bagge-Ravn, D.; Gadegaard, N.; Gram, L. *Langmuir* **2003**, *19*, 6912−6921.
(10) Roosjen, A.; van der Mei, H. C.; Busscher, H. J.; Norde, W. *Langmuir* **2004**, *20*, 10949−10955.
(11) Ostuni, E.; Chapman, R. G.; Liang, M. N.; Meluleni, G.; Pier, G.; Ingber, D. E.; Whitesides, G. M. *Langmuir* **2001**, *17*, 6336−6343.
(12) Tegoulia, V. A.; Cooper, S. L. *Colloids Surf., B* **2002**, *24*, 217−228.
(13) O'Toole, G.; Kaplan, H.; Kolter, R. *Annu. Rev. Microbiol.* **2000**, *54*, 49−79.
(14) Beloin, C.; Roux, A.; Ghigo, J. M. *Curr. Top. Mirobiol. Immunol.* **2008**, *322*, 249−289.
(15) Pratt, L.; Kolter, R. *Mol. Microbiol.* **1998**, *30*, 285−293.
(16) Riley, M. *Nucleic Acids Res.* **2006**, *34*, 1−9.
(17) Lederberg, J. *Microbiol. Today* **2004**, *31*, 116.
(18) Volle, C.; Ferguson, M.; Aidala, K. T.; Spain, E.; Núñez, M. E. *Colloids Surf., B* **2008**, *67*, 32−40.
(19) Hutter, J.; Bechhoefer, J. *Rev. Sci. Instrum.* **1993**, *64*, 1868−1873.
(20) Singh, M.; Kaur, N.; Singh, L. *Radiat. Phys. Chem.* **2010**, *79*, 1180−1188.
(21) Kuwahara, Y. *Phys. Chem. Miner.* **1999**, *26*, 198−205.
(22) Parker, J. L.; Cho, D. L.; Claesson, P. M. *J. Phys. Chem.* **1989**, *93*, 6121−6125.
(23) Okusa, H.; Kurihara, K.; Kunitake, T. *Langmuir* **1994**, *10*, 3577−3581.
(24) Núñez, M. E.; Martin, M.; Chan, P.; Spain, E. *Colloids Surf., B* **2005**, *42*, 263−271.
(25) Burks, G.; Velegol, S.; Paramonova, E.; Lindenmuth, B.; Feick, J.; Logan, B. *Langmuir* **2003**, *19*, 2366−2371.
(26) Cao, T.; Tang, H.; Liang, X.; Wang, A.; Auner, G.; Salley, S.; Ng, K. *Biotechnol. Bioeng.* **2006**, *94*, 167−176.
(27) Sheng, X.; Ting, Y. P.; Pehkonen, S. O. *J. Colloid Interface Sci.* **2007**, *310*, 661−669.
(28) Sheng, X.; Ting, Y. P.; Pehkonen, S. O. *J. Colloid Interface Sci.* **2008**, *321*, 256−264.
(29) Razatos, A.; Ong, Y.-L.; Boulay, F.; Elbert, D.; Hubbell, J.; Sharma, M.; Georgiou, G. *Langmuir* **2000**, *16*, 9155−9158.
(30) Ong, Y.-L.; Razatos, A.; Georgiou, G.; Sharma, M. *Langmuir* **1999**, *15*, 2719−2725.
(31) Lower, S. K.; Tadanier, C.; Hochella, M. F. *Geochim. Cosmochim. Acta* **2000**, *64*, 3133−3139.
(32) Atabek, A.; Liu, Y.; Pinzon-Arango, P. A.; Camesano, T. A. *Colloids Surf., B* **2008**, *67*, 115−121.
(33) Lau, P. C. Y.; Dutcher, J. R.; Beveridge, T. J.; Lam, J. S. *Biophys. J.* **2009**, *96*, 2935−2948.
(34) Touhami, A.; Jericho, M.; Boyd, J.; Beveridge, T. *J. Bacteriol.* **2006**, *188*, 370.
(35) Vadillo-Rodriguez, V.; Busscher, H.; Norde, W.; de Vries, J.; Dijkstra, R.; Stokroos, I.; van der Mei, H. *Appl. Environ. Microbiol.* **2004**, *70*, 5441−5446.
(36) Thorpe, A.; Peters, V.; Smith, J.; Nevell, T.; Tsibouklis, J. *J. Fluorine Chem.* **2000**, 378−345.
(37) Tsibouklis, J.; Stone, M.; Thorpe, A.; Graham, P.; Nevell, T.; Ewen, R. *Int. J. Adhes. Adhes.* **2000**, *20*, 91−96.
(38) Park, K. D.; Kim, Y. S.; Han, D. K.; Kim, Y. H.; Lee, E. H.; Suh, H.; Choi, K. S. *Biomaterials* **1998**, *19*, 851−859.
(39) Cheng, G.; Zhang, Z.; Chen, S.; Bryers, J. D.; Jiang, S. *Biomaterials* **2007**, *28*, 4192−4199.
(40) Rosenhahn, A.; Schilp, S.; Kreuzer, H. J.; Grunze, M. *Phys. Chem. Chem. Phys.* **2010**, *12*, 4275.
(41) Geoghegan, M.; Andrews, J. S.; Biggs, C. A.; Eboigbodin, K. E.; Elliott, D. R.; Rolfe, S.; Scholes, J.; Ojeda, J. J.; Romero-González, M. E.; Edyvean, R. G. J.; Swanson, L.; Rutkaite, R.; Fernando, R.; Pen, Y.; Zhang, Z.; Banwart, S. A. *Faraday Discuss.* **2008**, *139*, 85.
(42) Sides, P. J.; Faruqui, D.; Gellman, A. J. *Langmuir* **2009**, *25*, 1475−1481.
(43) Wei, Y.; Latour, R. A. *Langmuir* **2009**, *25*, 5637−5646.
(44) Sigal, G. B.; Mrksich, M.; Whitesides, G. M. *J. Am. Chem. Soc.* **1998**, *120*, 3464−3473.
(45) Estephan, Z. G.; Schlenoff, P. S.; Schlenoff, J. B. *Langmuir* **2011**, 6794−6800.
(46) Salloum, D. S.; Schlenoff, J. B. *Biomacromolecules* **2004**, *5*, 1089−1096.
(47) Knight, S. D.; Bouckaert, J. In *Structure, Function, and Assembly of Type 1 Fimbrae*; Lindhorst, T. K., Oscarson, S., Eds.; Topics in Current Chemistry; Springer: Berlin, 2009; Vol. *288*, pp 67−107.
(48) Allen, W. J.; Phan, G.; Waksman, G. *Curr. Opin. Struct. Biol.* **2012**, 1−7.
(49) Hartmann, M.; Lindhorst, T. K. *Eur. J. Org. Chem.* **2011**, 3583−3609.
(50) Choudhury, D. *Science* **1999**, *285*, 1061−1066.
(51) van der Aa, B.; Michel, R.; Asther, M.; Zamora, M.; Rouxhet, P.; Dufrêne, Y. *Langmuir* **2001**, *17*, 3116−3119.
(52) Wenner, J.; Williams, M.; Rouzina, I.; Bloomfield, V. *Biophys. J.* **2002**, *82*, 3160−3169.
(53) Lower, B. H.; Yongsunthon, R.; Vellano, F. P.; Lower, S. K. *J. Bacteriol.* **2005**, *187*, 2127−2137.
(54) Smith, S. B.; Cui, Y.; Bustamante, C. *Science* **1996**, *271*, 795−799.
(55) Camesano, T.; Abu-Lail, N. *Biomacromolecules* **2002**, *3*, 661−667.
(56) Clausen-Schaumann, H.; Seitz, M.; Krautbauer, R.; Gaub, H. E. *Curr. Opin. Chem. Biol.* **2000**, *4*, 524−530.

(57) Abu-Lail, N.; Ohashi, T.; Clark, R.; Erickson, H. *Matrix Biol.* **2006**, *25*, 175−184.
(58) Carrion-Vazquez, M.; Marszalek, P. E.; Oberhauser, A. F.; Fernandez, J. M. *Proc. Natl. Acad. Sci. U. S. A.* **1999**, *96*, 11288−11292.
(59) Capitani, G.; Eidam, O.; Glockshuber, R.; Grütter, M. G. *Microb. Infect.* **2006**, *8*, 2284−2290.
(60) Miller, E.; Garcia, T.; Hultgren, S.; Oberhauser, A. F. *Biophys. J.* **2006**, *91*, 3848−3856.
(61) Jass, J.; Schedin, S.; Fallman, E.; Ohlsson, J.; Uhlin, B.; Axner, O. *Biophys. J.* **2004**, *87*, 4271−4283.
(62) Müller, D.; Helenius, J.; Alsteens, D.; Dufrêne, Y. *Nat. Chem. Biol.* **2009**, *5*, 383−390.